SAND2016-0074J

Pickless Event Detection and Location: The Waveform Correlation Event Detection System (WCEDS) revisited

Stephen Arrowsmith, Chris Young, Sandy Ballard and Megan Slinkard
Sandia National Laboratories

Introduction

The standard paradigm for seismic event monitoring breaks the event detection problem down into a series of processing stages that can be categorized at the highest level into station-level processing and network-level processing algorithms (e.g., Le Bras and Wuster (2002)). At the station-level, waveforms are typically processed to detect signals and identify phases, which may subsequently be updated based on network processing. At the network-level, phase picks are associated to form events, which are subsequently located. Waveforms are typically directly exploited only at the station-level, while network-level operations rely on earth models to associate and locate the events that generated the phase picks. We refer to the class of methods that are based entirely on picks at the network level as 'pick-based methods', following Pesicek et al. (2014). Individual detection, association, and location algorithms, earth models, and wave propagation models have become increasingly sophisticated with time and pick-based methods remain the workhorse at operational seismic monitoring centers.

An alternative class of methods, which we refer to here as 'stack based methods', operates directly on the waveforms themselves, eliminating the step of deriving a set of picks at each station. Stack-based methods include a class of methods that can be referred to as Reverse Time Migration methods. These methods generally consist of a grid search over possible event hypotheses in space and time, where migration is used to focus waveform energy received at several stations back to the seismic source. Often, such methods are based on a few specific phases and require relatively simple travel-time predictions through earth models to align the energy (e.g., Kao and Shan, (2004), Baker et al. (2005)). A variant on this approach, which is less suitable for real-time event detection purposes, involves time reversal of the full wavefield using full wave modeling methods (e.g., Gajewski and Tessmer, (2005)). Another more empirical class of stack-based methods exists that is based on correlation using heavily processed stacks of observed data and therefore does not require a velocity model. Shearer (1994) outlined an approach for event detection that used a time-versus-distance image of the long-period teleseismic wavefield from known events as a matched filter to identify new events. His matched filter was constructed using an STA/LTA operator to heavily smooth the data and accentuate phase arrival times. Building on this work, Young et al. (1998; 1996) developed a method that they referred to as the Waveform Correlation Event Detection System (WCEDS). The WCEDS algorithm effectively fuses traditional detection, association, and location steps in a single algorithm. The method was subsequently implemented at a local scale by Withers et al. (1999). The WCEDS implementation described in

these earlier studies was based on the construction of synthetic stacks, rather than the empirical stacks described by Shearer (1994).

The main advantages of pick-based methods are related to speed, and to the fact that they work relatively well for detecting large events when using sparse networks. Stack-based methods typically involve a grid search over time and location to find events, and are therefore intrinsically slower. A major limitation of pick-based methods is that phase picks can be in error if the onset of the arrival is misidentified, which is relatively common when the signal-to-noise ratio is low. The phase of the pick can also be erroneous. Further, the association of picks can break down when there are a large number of individual events that are closely spaced in time and space, which is typical during aftershock sequences. For detecting relatively weak signals with a sensor network that is relatively dense, stack-based methods should outperform pick-based methods. Further, the speed advantage associated with pick-based methods is becoming increasingly irrelevant as computers continue to become faster and cheaper.

In this paper we revisit the stack-based method outlined by Shearer (1994), Young et al. (1998; 1996), and Withers et al. (1999) using a high density local and regional network in Utah. We compare the results obtained using our implementation of WCEDS with results from a pick-based method run by the University of Utah Seismograph Stations (UUSS), demonstrating that WCEDS detects many events that are not present in the UUSS catalog.

Method

The WCEDS algorithm is based on correlating processed incoming data against a historical time-versus-distance stack of the seismic wavefield. In contrast with traditional waveform correlation methods, seismograms are heavily processed using a bandpass filter and application of an STA/LTA operator (Withers et al., 1998). Traditional correlation methods are very powerful for detecting and locating repeating events but do not provide a general solution for broad-area regional monitoring. The STA/LTA operator has the advantage of enhancing phase arrivals and smoothing the time series to remove high-frequency effects that are strongly dependent on specific events and/or source-receiver paths. Furthermore, because the STA/LTA operator removes absolute amplitudes, site calibration errors are removed. Rather than exploiting wiggle-for-wiggle correlations, the WCEDS formulation exploits the time delays between phases, in addition to their smoothed temporal characteristics, as a function of source-receiver distance. In this paper we assume that the evolution of the STA/LTA processed waveforms varies only with distance. This is equivalent to assuming a 1D velocity structure, although we note that no velocity model is used in the formulation.

Assume that we have a set of N_S seismograms from different stations in a network that have been filtered by an STA/LTA operator, such that the i'th seismogram can

be written as $a_i(t) = P\left[x_i(t)\right]$, where $x_i(t)$ is the bandpass filtered vertical-component waveform for the i'th station and $P[\ldots]$ represents the STA/LTA operator. The objective is to detect and locate events on this set of processed seismograms in a moving time window.

The method is based on the construction of an empirical stack of observed STA/LTA processed seismograms from historical events recorded across a network. By using a catalog of events recorded by a network, we process historical data with an STA/LTA filter and construct a time-versus-distance stack of these data. The stack is stored as an $N_D \times N_T$ matrix, $\mathbf{M}$, where N_D is the number of distance bins and N_T is the number of time bins. Each element of $\mathbf{M}$ represents the mean value of STA/LTA from the entire catalog of historical data in a given time, distance bin. Based on the formulation described by Young et al. (1996) and Withers et al. (1999), $\mathbf{P}_w$ is calculated from:

$$\mathbf{P}_w = \left(\mathbf{M} \cdot \mathbf{D}\right)^T \cdot \mathrm{diag}\left(\mathbf{w}\right), \tag{1}$$

where $\mathbf{D}$ is a $N_T \times N_S$ matrix that contains all the processed data for an entire network in a moving time window such that each element represents the processed data at a given time for a given station; N_S is the number of stations; $\mathbf{P}_w$ is a $N_S \times N_D$ matrix containing elements, p_{ij}, that equal the product of the processed seismogram at a specific station with the stack at a given distance; and $\mathbf{w}$ is a vector of distance weights of length N_D. By parameterizing a region of study by a series of grid nodes, the correlation value, c, for a given grid node can subsequently be found by summing the relevant terms in $\mathbf{P}_w$ and normalizing:

$$c = \frac{1}{N_S} \sum_{k=1}^{N_S} \left(\frac{p_{i_k j_k}}{N_T} \right). \tag{2}$$

The relevant indices of terms in $\mathbf{P}_w$ for each grid node are stored in a lookup table. The $N_\phi \times N_\lambda$ matrix (where N_ϕ is the number of latitudes and N_λ is the number of longitudes) containing the correlations at all the grid nodes is referred to in this paper as $\mathbf{C}_w$. With $w_i = 1$, the dot product formulation in Equation (1) would account for spreading and attenuation as the STA/LTA amplitudes at each station, and in the stack, intrinsically include these effects. However, the averaging effect of Equation (2) can result in missing small events, because they may be only detected

by a few stations. To compensate for this, we weight by the inverse of the great-circle distance from the i'th station, Δ_i, such that $w_i = \Delta_i^{-1}$. This strategy is equivalent to down-weighting observations with large source-receiver separation that are less likely to have detected an event and is not an attempt to mimic real attenuation and spreading.

For a given origin time hypothesis $\left(t_0\right)$, event detection and location is implemented by finding peaks in $\mathbf{C}_w$ and determining if those peaks meet some criteria suitable for event detection. Because multiple events may be consistent with the same origin time hypothesis, we implement an iterative peak finding algorithm that is based on the approach outlined in Young et al. (1996). The algorithm begins by finding the latitude $\left(\phi_p\right)$ and longitude $\left(\lambda_p\right)$ of the largest peak in $\mathbf{C}_w$, and assigning an event hypothesis: $E_P = \left(\phi_P, \lambda_P, t_0\right)$. Next, a masking matrix with dimensions $N_S \times N_D$, $\mathbf{X}$, is defined to track station/distance pairs associated with the event hypothesis. Elements in $\mathbf{X}$ representing stations detecting the event, at their associated great-circle distances to E_P, are flagged. The correlation matrix, $\mathbf{C}_w$, is then recalculated using Equation 2, but neglecting terms in $\mathbf{P}_w$ with corresponding flags in $\mathbf{X}$, and the process is repeated until there are no more peaks above some threshold.

The full algorithm, which is represented as a flowchart in Figure 1, can be conceptualized as a nested loop where the outer loop iterates over different origin time hypotheses and the inner loop iterates over all location hypotheses at that origin time that exceed a correlation threshold. In addition, the algorithm includes logic that reconciles the results obtained at different origin time hypotheses. We use P_w and P to refer to weighted and unweighted products, and $\mathbf{C}_w$ and $\mathbf{C}$ to refer to correlation matrices evaluated using each type of product. The weighted product is used for event detection because it enables the detection of small events that may only be detected at a few stations; this is demonstrated in the Results section. The un-weighted product is used for event location because it intrinsically accounts for propagation times and amplitude reduction due to attenuation and spreading at the observing stations and does not bias the location through weighting by station distance. Only stations with products exceeding a specified threshold given the trial location obtained from the weighted correlation matrix are used for estimating the un-weighted correlation matrix for event location; this prevents the location being biased by noise observations. Event hypotheses generated for a given origin time hypothesis are compared with earlier event hypotheses to determine whether they represent new events or improved estimates of previous hypotheses; the associated logic is shown inside the red box in Figure 1. The final output of the algorithm is a catalog that contains a complete set of self-consistent event hypotheses.

Events with arrivals within a given processing time window but with origin times that are inconsistent with t_0 (i.e., where $t_0 <$ origin time $< t_0 + N_T dt$, with dt as the sampling rate) can result in artifacts in the calculated correlations. We have found that such artifacts can be effectively removed by comparing weighted correlation matrices with the corresponding un-weighted correlation matrices evaluated using detecting stations. When the origin-time hypothesis is correct, both weighted and un-weighted correlation maps are consistent with an event occurring in approximately the same location. However, for an incorrect origin-time hypothesis, weighted and un-weighted correlation maps look quite different because the peak un-weighted correlations occur systematically at time delays consistent with a more distant event yet the corresponding location solution is strongly down-weighted in the weighted correlations. Thus, by comparing locations obtained both with and without weighting we can identify artifacts by the difference in location between these two solutions – referred to as δ_1.

An estimate of the best event location is a natural byproduct of the event detection system described above. To obtain an estimate of the best point location, we note that the resolution of the peak location $\left(\phi_P, \lambda_P\right)$ is limited by the discretization of the grid, and increasing the number of nodes adds significant computational burden. To avoid these issues we resample $\mathbf{C}$ on a finer-resolution set of nodes and smooth the function using a 2D Gaussian filter to achieve finer location resolution without significant additional computational cost. This strategy is found to provide improved estimates of location, even when the original 2D function of $\mathbf{C}$ is spatially aliased. While the location estimates in WCEDS do not currently provide a formal statistical estimate of the associated uncertainty we plan to explore strategies for providing such assessments in future. Further enhancements that are planned for future work are discussed in the Discussion section.

This event detection scheme contains a number of parameters that must be tuned for a specific application based on an assessment of the desirable trade-off between the number of false alarms and the number of missed events. As such, WCEDS is no different from any other algorithm for seismic event detection, although we note that the number of parameters is lower than for most pick-based methods (e.g., Le Bras and Wuster, (2002)), partly because the detection, association, and location algorithms are effectively merged in WCEDS. The parameters that one might tune for a given application include the filter parameters, STA/LTA window durations, weighted network correlation threshold, the station correlation threshold, the move distance, and two thresholds that are designed to ensure that only the result from the origin time hypothesis most consistent with a specific event are stored (Δ_s and Δ_t).

Dataset and Construction of a 1D stack

In this paper we focus on the application of WCEDS to one day of data from the permanent regional seismic network operated by the University of Utah Seismograph Stations (UUSS), coinciding with the period of time that USArray Transportable Array (TA) seismic stations was deployed in Utah. We use data from 2007 and 2008 to construct our historical time-versus-distance stack. During this time period, there were seismic stations at a total of 140 locations in Utah (Figure 2). The precise constellation of stations changed with time as TA stations were moved. The UU network is distributed along the N-S trend of seismicity, while the TA network is distributed as a semi-regular grid across the region. In 2007 and 2008 there are a total of 5595 events listed in the UUSS catalog (Figure 2). The earthquake magnitudes are small, ranging from <0 to 3.93 with a median magnitude of 1.38.

We use all 77 earthquakes with magnitudes greater than 2.5 in the UUSS catalog to generate the 1D stack represented previously by $\mathbf{M}$ (Figure 3). We note that none of these events are present in the 1-day period in which we have tested WCEDS. Since large events should be more precisely located than small events, and have better SNR, we use these events in constructing $\mathbf{M}$. Errors in the stack will map to errors in our resultant event catalogs, although by using a large number of observations in generating the stack, errors should be reduced via averaging. Based on all event-receiver paths from the 77 events, a total of 8951 STA/LTA processed waveforms are used to construct the stack, which is shown in Figure 3. We process data using a simple recursive STA/LTA filter (Withers et al., 1998). First, the data are filtered from 0.5 to 4 Hz with a bandpass Butterworth filter. Next, the data are filtered using STA/LTA filter parameters of STA=3s, LTA=60 s (tuned following Trnkoczy (2012)). The matrix, $\mathbf{M}$ is formed by averaging all STA/LTA values in time/distance bins. We choose time bins of duration equal to 0.05 s and distance bins of 10 km. Slices through $\mathbf{M}$ at every 10 km interval are shown in Figure 3. Three dominant phases are clearly seen, corresponding to Pg, Pn, and Lg. The Pg/Pn crossover distance is ~200 km, with a very sharp onset at closer distances. The Lg phase is characterized by a much more emergent onset. We emphasize that no assumptions are made about what phases are present: they just emerge from the stack according to how they are represented in the observed data and with the appropriate relative amplitudes. This is very different from pick-based models, where a decision must be made about what phases to use and travel time curves for each phase must be developed or obtained.

Application of WCEDS and comparison with the UU catalog

For evaluating the WCEDS algorithm described above, we show the results obtained by applying the method to 1-day of data (09/18/2007 00:00 – 09/19/2007 00:00) at UU network stations, allowing direct comparison with the UUSS catalog. The selected day contained 47 events in the UUSS catalog, with magnitudes between

0.42 and 1.74 and the majority of events (43) forming a tight geographic cluster around 39.43°N, 111.21°W near the center of the region of study.

A number of events in the UUSS catalog can only be detected on the basis of Equations 1 and 2 when using the distance-weighting operator, $\mathbf{w}$. The benefit of using this operator is demonstrated in Figure 4; a correlation peak associated with an event in the UUSS catalog at 39.4°N, 111.2°W is enhanced when distance weighting is applied. The event can be observed as a local peak in the network correlation time series in this case but for other cases there is no evidence of the event until distance weighting is applied. Because distance weighting can enhance the detection of small events, the peak distance-weighted network correlation is used as the primary event detection criteria as described above and in Figure 1.

The calculated value of $\max\left(\mathbf{C}_w\right)$ for the 1-day period is shown in Figure 5. The distribution of values over the 1-day period varies between 0.01 and 0.06 with a mean of 0.019; the largest events are readily detected by setting a threshold deep in the tail of the distribution (>0.04), while reducing the threshold naturally results in detecting more events at the cost of increasing the false alarm rate. A comprehensive analysis of the probability of detection and false alarm is beyond the scope of this paper, our goal is to evaluate how the results obtained using the WCEDS methodology described above compare with the UUSS catalog for the period of study. To this end, we note that each UUSS event directly corresponds to a peak in $\max\left(\mathbf{C}_w\right)$. However, there are many more peaks than events in the UUSS catalog. Furthermore, the 47 events in the UUSS catalog do not correspond to the 47 largest peaks in Figure 5. In particular, one of the UUSS events corresponds to a relatively low amplitude peak, while there are numerous larger peaks that are not associated with events in the UUSS catalog. This suggests some difference in the sensitivity of WCEDS and the pick-based method used by UUSS for detecting events.

Varying the thresholds required by WCEDS we can experiment with different scenarios. As mentioned previously, the most important threshold is the peak distance-weighted network correlation threshold. The secondary thresholds (move distance, Δ_s, and Δ_t) enable us to reject false events associated with an incorrect origin-time hypothesis and have been tuned to minimize such false events without rejecting real events in the period of study. We use values of $\delta_{\mathbf{l}_{\max}}$ = 20 km, Δ_s = 50 km, and Δ_t = 10 s and explore below the effects of varying the peak distance-weighted network correlation threshold, which has a much stronger influence on the results. By choosing the minimum threshold such that all events in the UUSS catalog are detected (c = 0.0285), we find 128 new events. By manually reviewing each of these events through plotting record sections, we find that 49 of these new events do not have clear arrivals at more than one station with a moveout consistent with the derived location and origin time. Thus, with a threshold of 0.0285 there are at least 79 new events detected that are not reported in the UUSS catalog with a

possible false alarm rate of 49/day (we note that some of these false alarms may be real events that are only detected at one station or else are buried in noise). However, raising the threshold to c = 0.035, we miss only one UUSS event and detect 61 new events, of which 9 are possible false alarms. By setting the threshold such that we obtain no possible false alarms, we still detect more events than are listed in the UUSS catalog but we start missing additional UUSS events. For example, with a threshold of 0.04 we obtain 70 events, of which 43 are in the UUSS catalog. Examples of events detected by WCEDS at different peak distance-weighted correlations are shown in Figure 6.

To gain an understanding of the effect of station coverage on event detection with WCEDS, we show in Figure 7 how the number and distribution of detecting stations influences the detection of an example event that was observed out to ~50 km. The event is present in both UU and WCEDS catalogs with consistent event hypotheses (Location = 39.43°N, 111.21°W; Origin time = 2007/09/18 17:00:50.89). The event magnitude in the UU catalog is 1.06; there are 9 stations with visible signals in the UU network. By sequentially removing stations with observed waveforms it is seen how the peak correlation decreases as detecting stations are removed. With two local stations we could detect the event but the threshold would need to be set at approximately 0.02; such small events are likely associated with a large number of correlation peaks in the 1-day period studied in this paper (Figure 5). While the example in Figure 7 demonstrates that WCEDS is capable of detecting events observed by very few stations, a more comprehensive study of the network false alarm rate than is provided above would be desirable before running WCEDS at such a sensitive level.

A comparison of the locations of events detected by WCEDS, using a threshold of 0.0285, and the locations of events in the UUSS catalog is shown in Figure 8. As noted before, the largest concentration of events in the UUSS catalog is confined to a relatively tight cluster centered on ~39.6°N, 111.2°W. This cluster is associated with 137 events in the WCEDS catalog, suggesting that WCEDS is detecting a number of additional events associated with an active fault system during the period of study. Additional clusters of WCEDS events can be identified, suggestive of additional repeaters during the 1-day period. Some of these clusters are associated with only one or no events in the UUSS catalog.

Discussion and Conclusions

The stack-based method presented in this paper, which builds on an earlier work by Shearer (1994), Young et al. (1996), and Withers et al. (1999), has the advantage that it can detect events across a network without requiring phase picks or a velocity model. The only requirement is a set of prior events with high-quality locations and origin times from which to construct an empirical time-versus-distance image of the processed seismic wavefield. By processing the data with an STA/LTA operator, the image is relatively insensitive to the precise source

mechanism or location and is more representative of the travel-time characteristics of the seismic phases in a given region.

It is worth noting that the earlier work on WCEDS did not result in the method becoming widely adopted, or motivate significant further research and development of the algorithm. In part, we believe this was due to the limitations of widely available computational resources at the time, which required a relatively sparse resolution on origin time, and on the time-versus-distance image, compared with what we have implemented in this paper. Further, the earlier studies were implemented primarily on sparse global networks, with only the study by Withers et al. (1999) focused on a (relatively sparse) local network. In this study we have tested the methodology on a dense regional seismic network using a much finer resolution on origin time and the time-versus-distance image. Further, we use an empirical time-versus-distance image, rather than a synthetic time-versus-distance image as utilized by Young et al. (1996) and Withers et al. (1999). The advantage of an empirical image is that it exploits the actual temporal characteristics of the different seismic phases in a given region; the disadvantage is the need for prior data to construct such an image. Another modification implemented here, which was not implemented in earlier studies, is the use of both distance-weighted and unweighted images for enhancing the detection of weak events and mitigating artifacts associated with events in the record that occur at a different origin time than the one under test. As a result of some of these differences, the results obtained here are much more compelling than in previous studies and clearly demonstrate the improved sensitivity of WCEDS, compared with a traditional pick-based method, to relatively low-magnitude events with a dense seismic network. Using WCEDS we are able to detect many events that were not detected in the UUSS system, even using a high threshold such that the false alarm rate is zero in the 1-day period. By accepting a higher false alarm rate, the number of real events detected increases significantly, but at the cost of requiring further analyst review. Further research is required to develop improved strategies to reduce this burden and enable one to drive down the detection limit further; our results suggest it is possible to detect very small events detected by only one or two stations with this method.

The method outlined here contains some limitations that will be addressed in future work. For example, we currently only utilize vertical-component seismograms but note that the use of three-component data should further enhance the detection of weak events, especially by incorporating information from phases that are not well observed on vertical component seismograms, such as Sn. A second limitation is the absence of depth in the parameterization scheme; depth variations will affect the character of the regional wavefield and these effects are currently averaged out via the stacking procedure. In this paper we focus on the application of WCEDS to a region with shallow seismicity, thus depth effects are not expected to be significant. A third limitation is the assumption of a 1D stack, which does not account for lateral heterogeneity across a region. These limitations are not explored in detail in this paper and are left for future research.

References

Baker, T., Granat, R., & Clayton, R. W. (2005). Real-time Earthquake Location Using Kirchoff Reconstruction. *Bull. Seism. Soc. Am., 95*, 699 - 707. doi:10.1785/0120040123

Gajewski, D., & Tessmer, E. (2005). Reverse modelling for seismic event characterization. *Geophys. J. Int., 163*. doi:10.1111/j.1365-246X.2005.02732.x

Kao, H., & Shan, S.-J. (2004). The Source-Scanning Algorithm: mapping the distribution of seismic sources in space and time. *Geophys. J. Int., 157*, 589 - 594. doi:10.1111/j.1365-246X.2004.02276.x

Le Bras, R., & Wuster, J. (2002). *IDC Processing of Seismic, Hydroacoustic, and Infrasonic Data*. Retrieved from

Pesicek, J. D., Child, D., Artman, B., & Cieslik, K. (2014). Picking versus stacking in a modern microearthquake location: Comparison of results from a surface passive seismic monitoring array in Oklahoma. *Geophysics, 79*(6). doi:10.1190/GEO2013-0404.1

Shearer, P. M. (1994). Global seismic event detection using a matched filter on long-period seismograms. *J. Geophys. Res., 99*, 13713 - 13725.

Trnkoczy, A. (2012). *Understanding and parameter setting of the STA/LTA trigger algorithm*. Retrieved from

Withers, M., Aster, R., & Young, C. (1999). An Automated Local and Regional Seismic Event Detection and Location System Using Waveform Correlation. *Bull. Seism. Soc. Am., 89*(3), 657 - 669.

Withers, M., Aster, R., Young, C., Beiriger, J., Harris, M., Moore, S., & Trujillo, J. (1998). A Comparison of Select Trigger Algorithms for Automated Global Seismic Phase and Event Detection. *Bull. Seism. Soc. Am., 88*(1), 95 - 106.

Young, C., Beiriger, J., Moore, S., Trujillo, J., & Harris, M. (1998). *The Waveform Correlation Event Detection System Project, Phase II: Testing with the IDC Primary Network*. Retrieved from

Young, C., Beiriger, J., Trujillo, J., Withers, M., Aster, R., Astiz, L., & Shearer, P. M. (1996). *WCEDS: A Waveform Correlation Event Detection System*. Retrieved from

Young, C., Harris, M., Beiriger, J., Moore, S., Trujillo, J., Withers, M., & Aster, R. (1996). *The waveform correlation event detection system project phase 1: issues in prototype development and testing*. Retrieved from

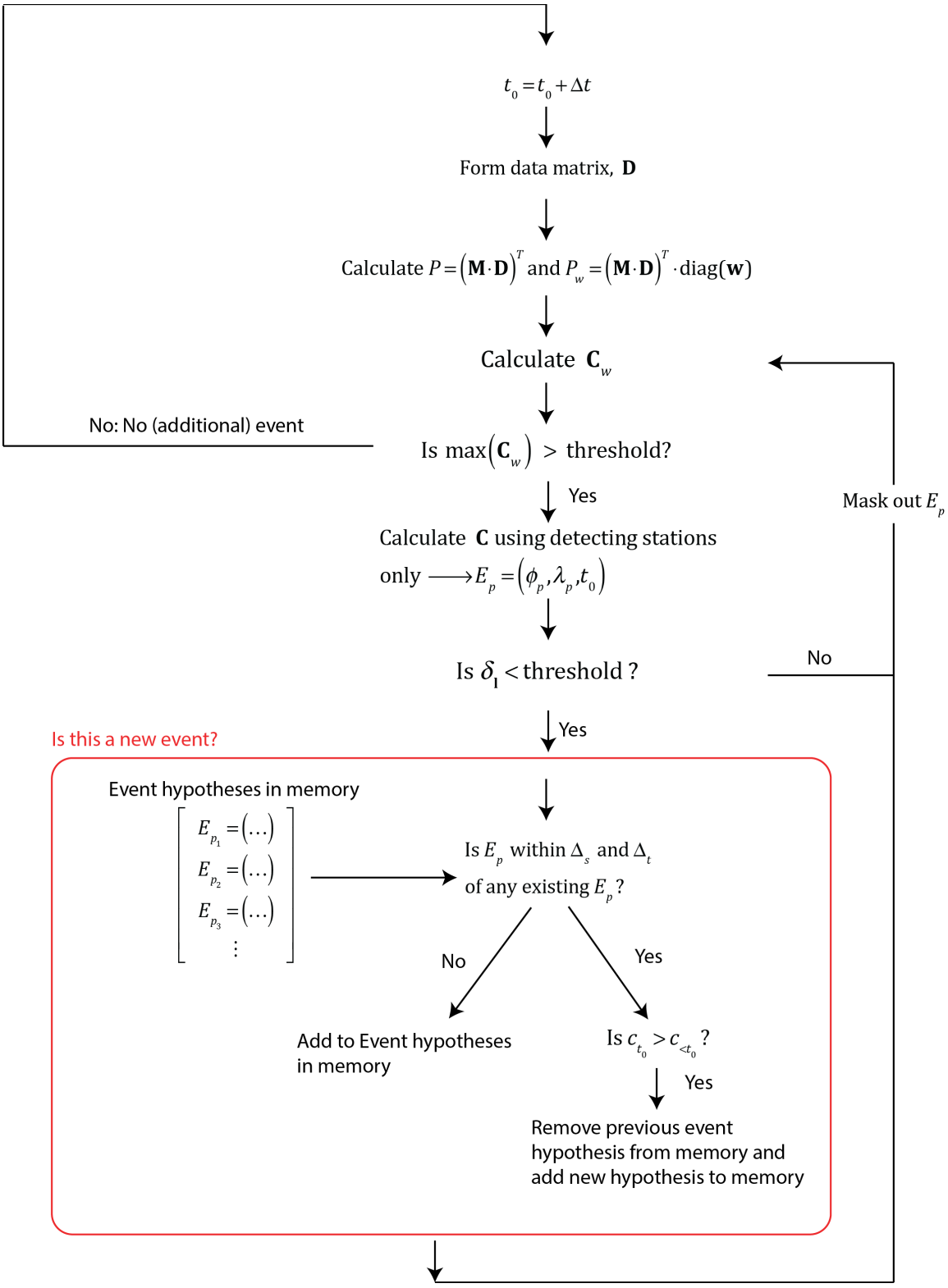

Figure 1. Flowchart illustrating the implementation of WCEDS described in this paper.

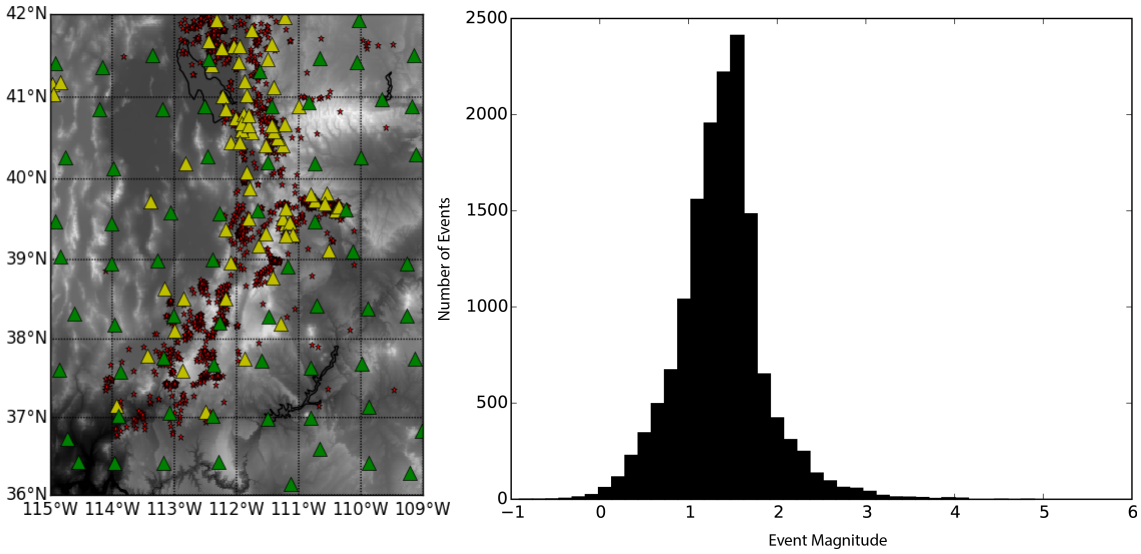

Figure 2. (left) Map showing locations of 140 broadband seismic stations in Utah in 2007 and 2008 (yellow triangles are UU stations, green triangles are TA stations) and locations of seismic events in the UUSS seismic catalog for the same two-year time interval (red stars). (right) Distribution of magnitudes of all seismic events in the two-year time interval.

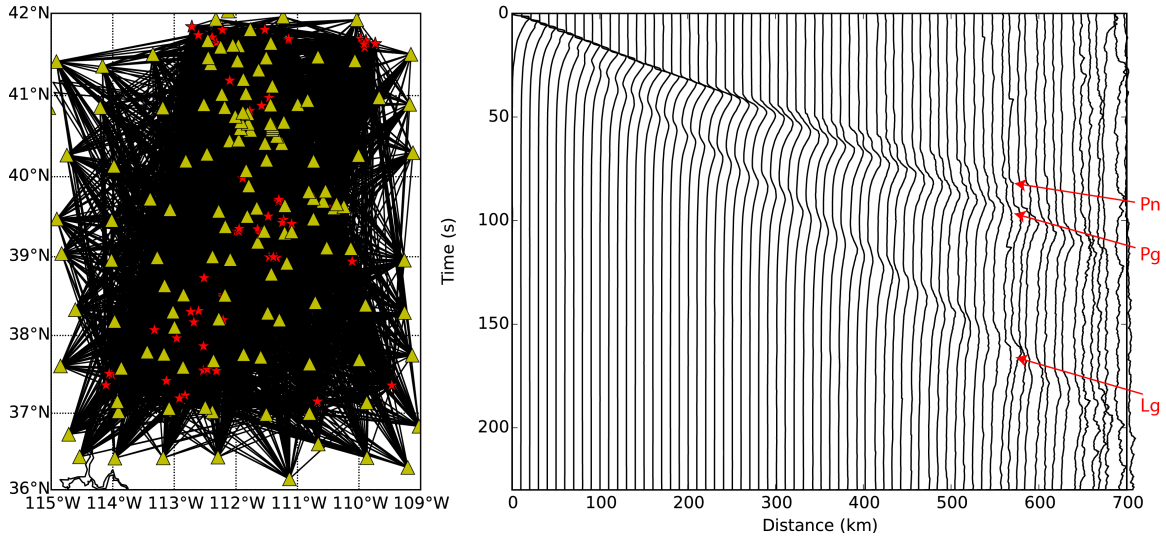

Figure 3. The 1D STA/LTA stack used for event detection in this study. The left panel shows a map of the 8951 event-station paths that were used to construct the stack. The event-station paths were formed from 77 M>2.5 events (red stars), where each event was recorded on a subset of the 140 stations (yellow triangles). The right panel shows slices through the stack matrix at intervals of 10 km. The Pn, Pg, and Lg arrivals are labeled.

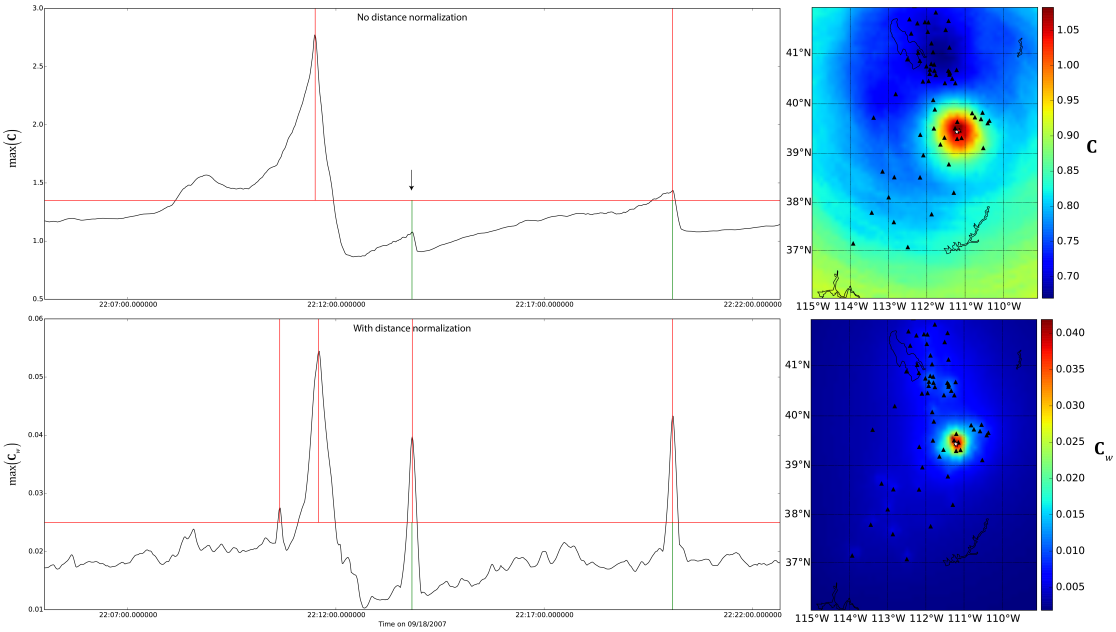

Figure 4. An event in the UU catalog that is missed without distance normalization, but detected with distance normalization. The left panel shows $\max(\mathbf{C})$ as a function of time both without (top) and with distance normalization (bottom). The right panels show time snapshots of $\mathbf{C}(\phi,\lambda)$ at the UU origin time, denoted by the black arrow in the left panel. In the left panel, green lines are origin times for events from the UU event catalog and red lines are origin times of events detected by WCEDS.

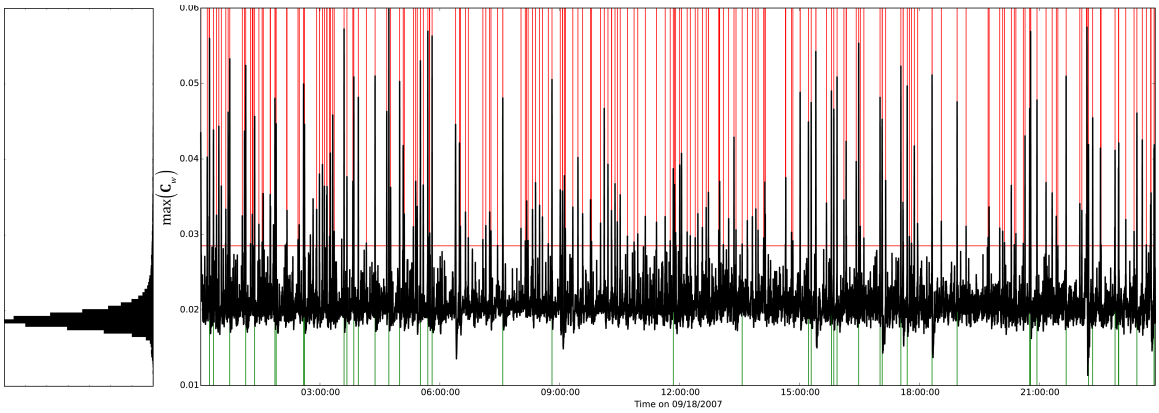

Figure 5. A comparison between the WCEDS correlation function and origin time estimates using data from the UU stations on 09/18/2007. Green lines are origin times for all 47 events from the UU event catalog and red lines are origin times of events detected by WCEDS given a threshold of 0.028. The distribution of $\max\left(\mathbf{C}_w\right)$ is shown for the full 1-day processing run in the left panel. The correlation functions obtained by applying WCEDS to both UU and TA stations together were virtually identical but the correlation values were shifted slightly lower.

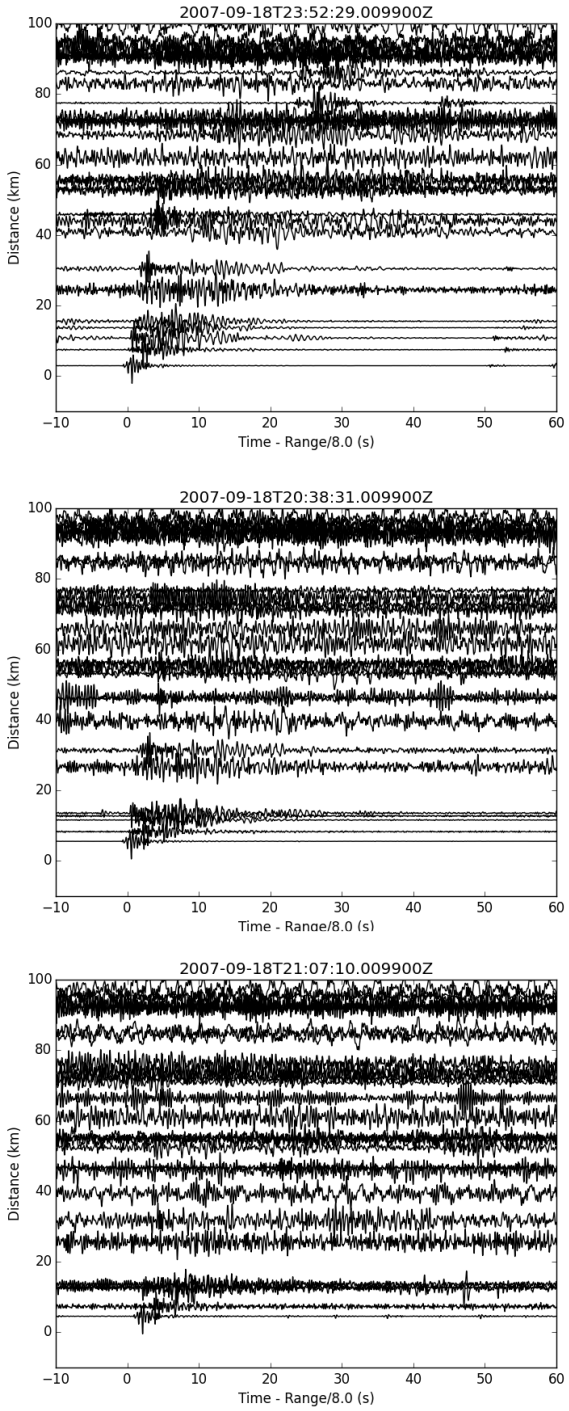

Figure 6. Record sections of three example events detected by WCEDS. The top panel shows an event that is also detected in the UUSS catalog. The center and lower panels show two new events found by WCEDS. The corresponding peak distance-weighted network correlations are, from top to bottom, 0.043, 0.043, and 0.027.

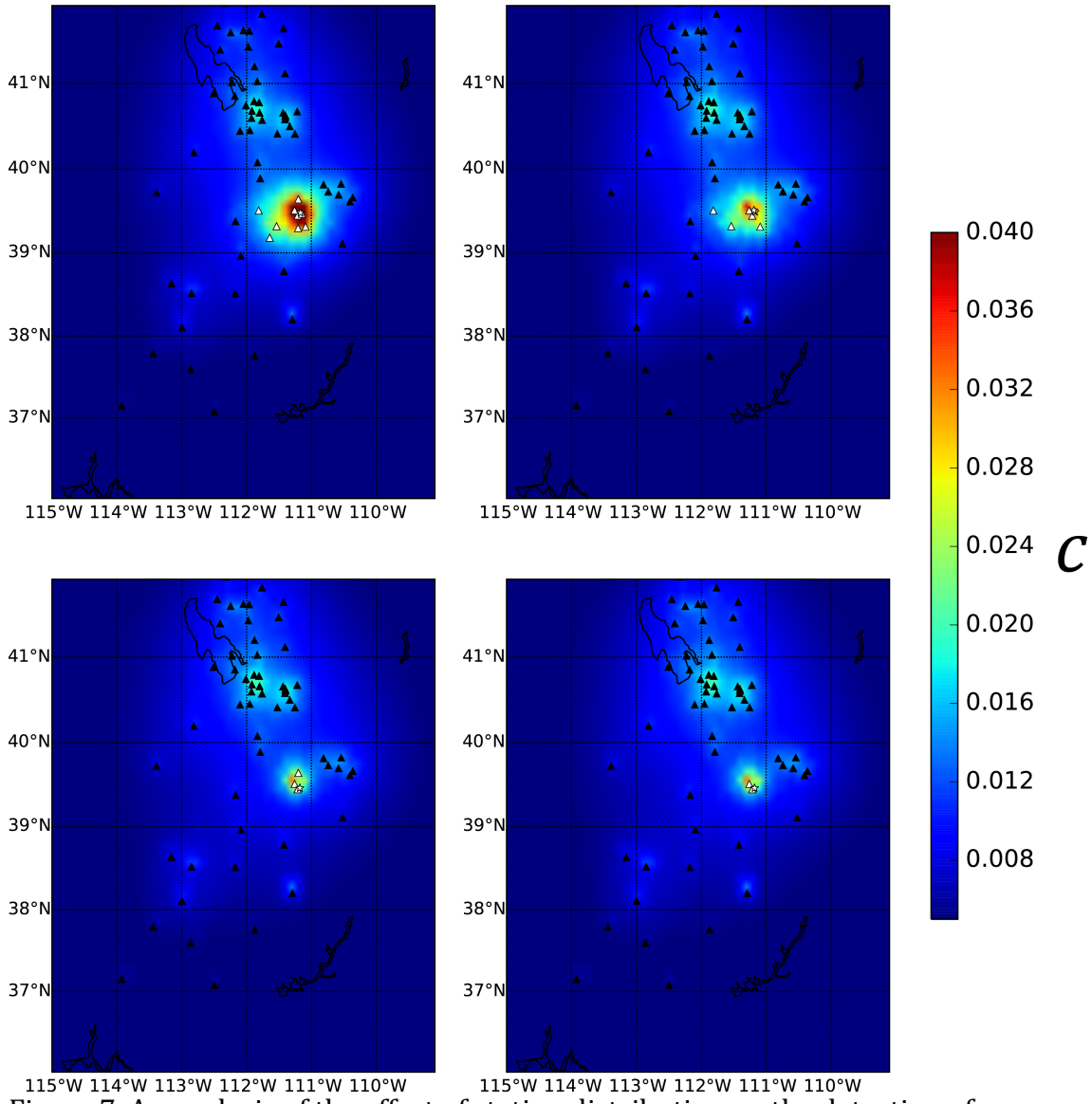

Figure 7. An analysis of the effect of station distribution on the detection of a magnitude 1.06 event in central Utah. The top left panel shows the WCEDS solution using the full UU networkt. Stations that have visible recordings are shown by white triangles and other stations are shown by black triangles. The remaining panels show the corresponding solution for reduced sets of detecting stations: five (top right), three (bottom left), and two (bottom right).

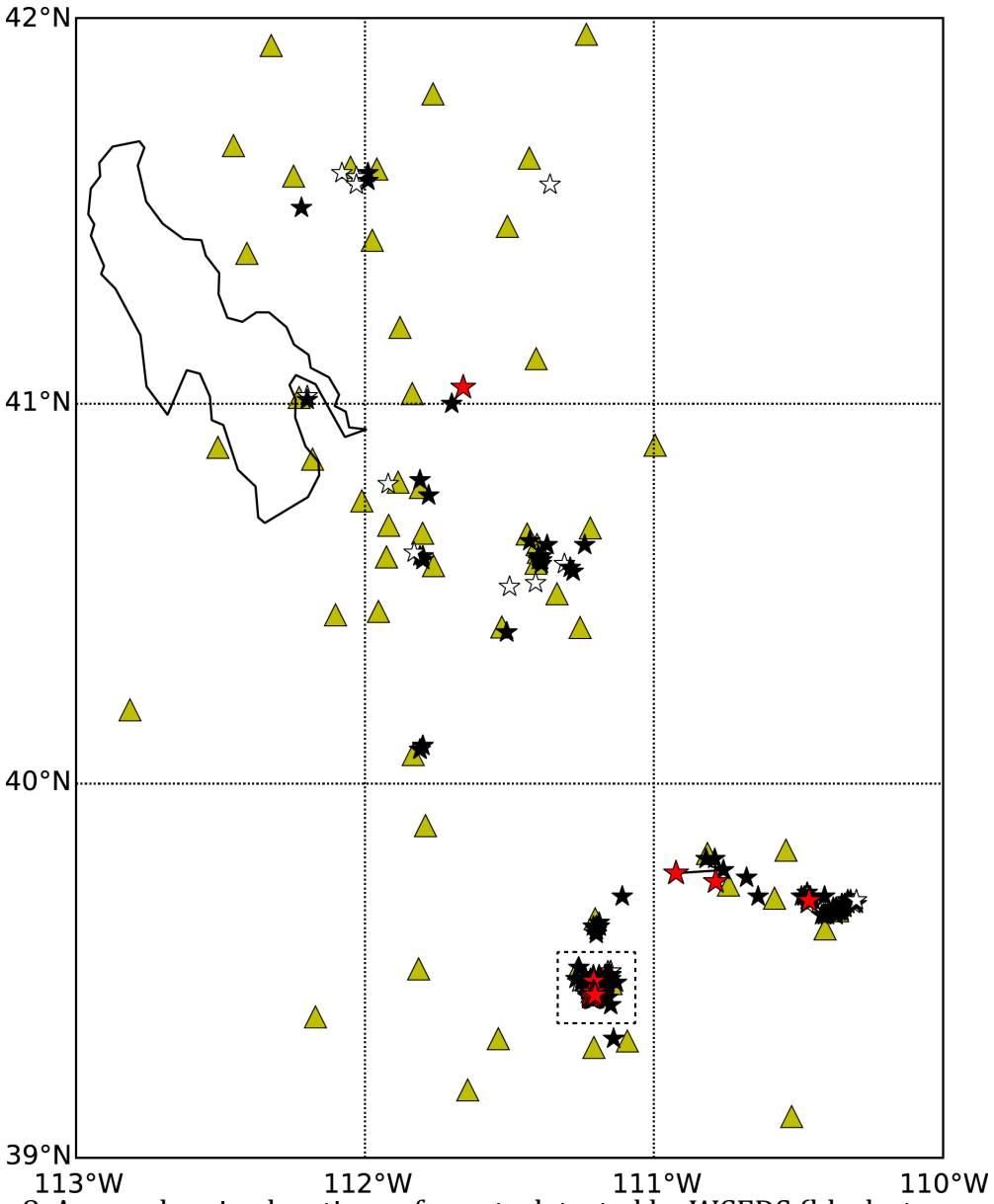

Figure 8. A map showing locations of events detected by WCEDS (black stars are WCEDS events determined to be real by an analyst; white stars are possible false alarms) with a threshold of 0.0285, locations of events in the UUSS catalog (red stars), and UU network stations (yellow triangles). The area denoted by the dashed black box contains 43 events in the UUSS catalog and 137 events in the WCEDS catalog. The largest discrepancy between a WCEDS location and UUSS location is 14 km, and is shown by the black line; the mean discrepancy in location is 3.8 km.